CrystEngComm

PAPER



Cite this: *CrystEngComm*, 2018, **20**, 3505

# Room-temperature synthesis of χ-$Al_2O_3$ and ruby (α-Cr:$Al_2O_3$)

Fernando D. Cortes-Vega,[ab] Wenli Yang,[c] J. Zarate-Medina,[b] Stanko R. Brankovic,[c] José M. Herrera Ramírez[d] and Francisco C. Robles Hernandez *[ace]

Received 7th March 2018,
Accepted 21st May 2018

DOI: 10.1039/c8ce00360b

rsc.li/crystengcomm

In this work, we present a unique crystal growth synthesis of χ-$Al_2O_3$ accompanied with α-Cr:$Al_2O_3$ at room temperature. Raman spectroscopy and additions of $Cr_2O_3$ are key to identifying α-Cr:$Al_2O_3$ in trace amounts by the room temperature synthesis of ruby (α-Cr:$Al_2O_3$). The presence of this phase is further confirmed with HRTEM. The raw materials are pseudoboehmite and $Cr_2O_3$ that are treated mechanochemically for the successful synthesis of ruby and χ-$Al_2O_3$. A thermal analysis approach is provided to explain the significant temperature reduction for the complete transformation to α-Cr:$Al_2O_3$ during annealing. The α-Cr:$Al_2O_3$ synthesized at room temperature acts as the seed or hetero site for nucleation and is responsible for a temperature drop of approximately 200 °C (up to 867 °C). This material is ideal for optics, photonics, defense, energy storage and harvesting, among other strategic applications.

## Introduction

Alumina is one of the most abundant and widely used ceramics, having a wide range of applications from cookware to catalysis, electronics, medical, optics, aerospace, and defense, among others.[1–4] The outstanding hardness and stability of alumina(s) ($Al_2O_3$) allow it to be used under extreme environments such as high temperatures, highly corrosive environments, compressive stresses, *etc.* These characteristics make alumina desirable for many uses where the word nano is a common prefix.[5–8] Naturally occurring alumina is the second hardest material, just after diamond. α-$Al_2O_3$ and $Cr_2O_3$ form a complete solution in solid and liquid states.[1,9,10] Their solid solution is commonly known as ruby and forms by the substitution of $Al^{3+}$ for $Cr^{3+}$ in octahedral sites.[10,11] The formation of the solid solution involves a small expansion of the α-$Al_2O_3$ lattice, owing to the comparatively larger ionic radius of $Cr^{3+}$.[12]

Ruby is well known for its resonant luminescence bands ($R_1$ and $R_2$) that are easily detectable with Raman spectroscopy. These bands are known for their sensitivity to shift with temperature and pressure.[13–17] This characteristic makes ruby a highly desirable material, not only as a gemstone, but also as a sensor with applications under extreme conditions (*e.g.* pressure and temperature). Conventionally, ruby is synthesized out of α-$Al_2O_3$ (corundum) with $Cr^{3+}$ additions at temperatures of at least 1200 °C. Here we present a unique methodology to synthesize significant amounts of this phase at room temperature. However, for the complete transformation, one needs to heat treat the material. Yet, the transformation occurs at approximately 193 °C below the typical phase transition temperature. The process presented herein is able to synthesize χ-$Al_2O_3$ at room temperature using pseudoboehmite as the precursor. During the milling process, full dehydroxylation occurs at room temperature. This process is usually observed at temperatures between 300 and 500 °C.[18–26] Hitherto, for the first time, we demonstrated that this transformation can be accomplished at room temperature, purely by milling, in the absence of other $Al_2O_3$ phases such as θ, γ, κ, and δ.

We report the room temperature phase transformation of pseudoboehmite to χ-$Al_2O_3$ and ruby (α-Cr:$Al_2O_3$) based purely on milling in SPEX. The complete transformation to χ-$Al_2O_3$ is evident in the sample milled for approximately 30 h. In the milled samples, one can observe the presence of α-Cr:$Al_2O_3$. This phase is identifiable in the sample milled for as little as 5 h. However, the presence of α-Cr:$Al_2O_3$ is in small fractions, perhaps traces that are undetectable by XRD. The major novelty of our work consists on the addition of traces of $Cr_2O_3$ to synthesize ruby that can be detected by

[a] *Department of Mechanical Engineering Technology, University of Houston, Houston, TX, USA. E-mail: fcrobles@uh.edu*
[b] *Instituto de Investigación en Metalurgia y Materiales, Universidad Michoacana de San Nicolás de Hidalgo, Ciudad Universitaria, Michoacán, Mexico*
[c] *Department of Electrical and Computer Engineering, University of Houston, Houston, TX, USA*
[d] *Centro de Investigación en Materiales Avanzados, CIMAV, Chihuahua, Mexico*
[e] *Department of Materials Science and Engineering, University of Houston, Houston, TX, USA*

Raman spectroscopy. The detection of parts per million amounts of ruby is possible with Raman. This work demonstrates four major findings: the room temperature synthesis of i) $\chi$-$Al_2O_3$ and ii) $\alpha$-Cr:$Al_2O_3$ with SPEX, iii) the changes in phase transformation energy requirements and iv) a 193 °C drop in phase transformation temperature from $\chi$-$Al_2O_3$ to $\alpha$-$Al_2O_3$.

## Results and discussion

Fig. 1 shows the XRD spectra of the raw pseudoboehmite and the milled samples. Room temperature milling is capable of fully transforming pseudoboehmite into $\chi$-$Al_2O_3$ for times as short as 30 h. $\chi$-$Al_2O_3$ is a unique phase not well investigated and it is not typically found in non-heat treated samples. The pseudoboehmite shows the following 7 diffraction planes: (020), (120), (031), (200), (151), (002) and (251) that match with the XRD reference pattern (21-1307 JCPDS). Yet, (020) is slightly shifted toward lower angles in comparison with the crystalline boehmite. This shift is attributed to the presence of interlayers of water.[27–29] Therefore, due to the excess of water in the lattice we conclude that we do not have boehmite; instead, we have pseudoboehmite.

Pseudoboehmite has an orthorhombic crystalline structure with the oxygen in anionic arrangements and the aluminum cations in the octahedral sites. The relatively low concentration of $Cr_2O_3$ is untraceable by XRD. Fig. 1 shows evidence of the effects of mechanical milling time on the broadening of the reflections which is translated into a reduction in grain size. This effect is observed even at short milling times (5 h). What is unique is the transformation to $\chi$-$Al_2O_3$ at room temperature. In the literature, $\chi$-$Al_2O_3$ has been reported at temperatures between 300 and 500 °C.[30–32]

The identification of $\chi$-$Al_2O_3$ is carried out by comparing the experimental XRD with that reported in 13-0373 JCPDS. In the sample milled for 30 h, the pseudoboehmite is no longer discernible; instead, the $\chi$-$Al_2O_3$ phase is the only observable phase. This is the first report, as far as we are aware, on this transformation at room temperature.

The typical pseudoboehmite reflections corresponding to the planes (151) and (251) are no longer present after 10 h of milling which results from the transformation to $\chi$-$Al_2O_3$. However, the reflections become predominant after 30 h of milling. This phase transformation path is unique to mechanical milling[33] and the obtained $\chi$-$Al_2O_3$ does not have traceable amounts of other phases such as $\theta$, $\gamma$, $\kappa$, and $\delta$. Those phases are typically found when the transformation is done using other precursors and heat treatments. In parallel experiments, when we heat treat our samples, the transformation follows the following path: pseudoboehmite → $\delta$-$Al_2O_3$ → $\alpha$-$Al_2O_3$. In the milled samples, the transformation is as follows: pseudoboehmite → $\chi$-$Al_2O_3$ → $\alpha$-$Al_2O_3$. This means no evidence of $\gamma$-$Al_2O_3$ is observed.

Fig. 2 shows the Raman spectra of the analyzed samples in the range of 300 $cm^{-1}$ to 800 $cm^{-1}$. The raw sample showed three active modes ($A_g$ + $B_{1g}$ + $B_{3g}$) assigned to the most prominent bands of pseudoboehmite detected at ~364 $cm^{-1}$, 488 $cm^{-1}$ and 683 $cm^{-1}$.[34] Only one vibrational mode ($A_{1g}$) for $Cr_2O_3$ is discernible at ~563 $cm^{-1}$,[8] the relative intensity of which is attributed to the relatively low concentration.

The mechanical milling affected the structure of pseudoboehmite, leading to the shift of its vibrational modes to lower frequencies. This shift is evident in milling times as short as five hours. At longer milling times, the intensity of the vibrational modes of pseudoboehmite decreases, which suggests a reduction in the crystal quality or a grain refining effect. From Fig. 2, it is observed that the $A_{1g}$ band of $Cr_2O_3$ changes with the milling time. This band is detected in the raw sample pseudoboehmite + $Cr_2O_3$ and in milled samples for up to 10 h. After 20 h of milling, the band of $Cr_2O_3$ is no longer traceable. Here we associate the absence of the $A_{1g}$ mode with the rupture of $Cr_2O_3$ that generates $Cr^{3+}$ ions and substitute $Al^{3+}$ in the host lattice. In order to identify the effects of $Cr_2O_3$, the Raman range needs to be changed to a luminescence range for ruby which is between 4300 and 4500 $cm^{-1}$ (Fig. 3a).

Fig. 3a shows the Raman analysis in the range of 4300 $cm^{-1}$ to 4500 $cm^{-1}$ which is the location where we expect to observe the luminescence bands $R_1$ and $R_2$. The presence of those bands demonstrates that $Cr_2O_3$ drove the synthesis of

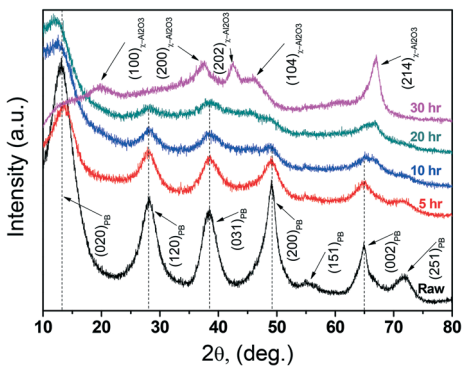


Fig. 1 Diffraction patterns of the raw and milled samples. PB and $\chi$-$Al_2O_3$ stand for pseudoboehmite and chi-alumina, respectively.

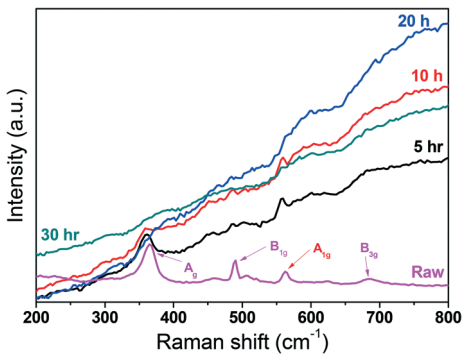


Fig. 2 Raman spectra of raw and milled samples with an excitation line of 532 nm. All the identified bands are associated with pseudoboehmite, except for $A_{1g}$ that is typical of $Cr_2O_3$.

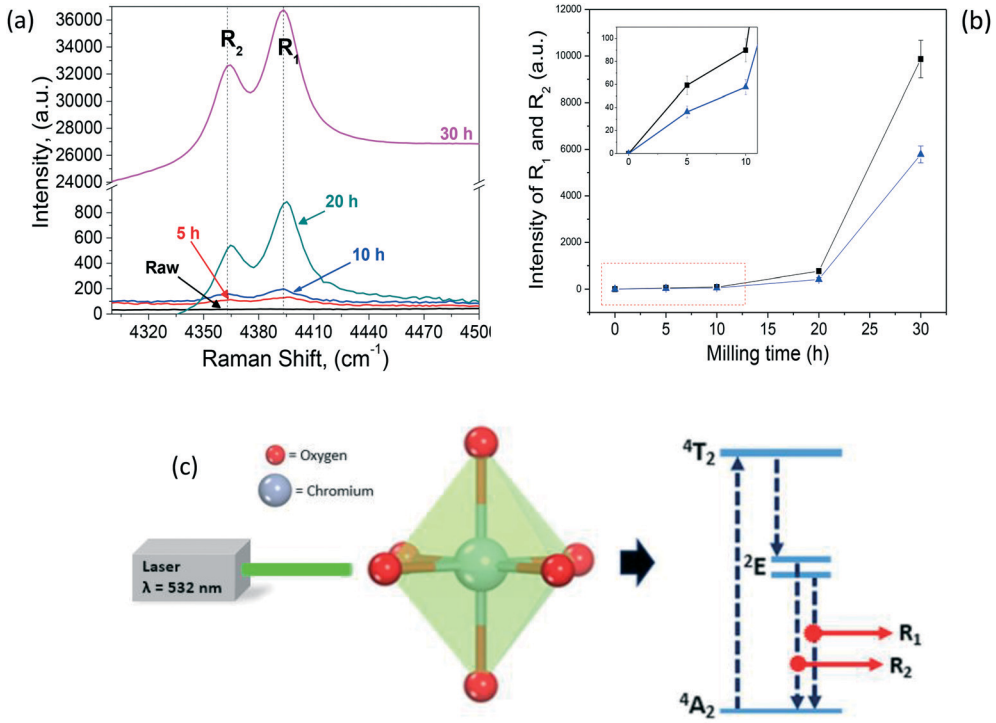


**Fig. 3** (a) Raman spectra of raw and milled samples for up to 30 h and (b) change of intensity ($R_1$ and $R_2$) as a function of milling time. Note the difference in intensity between the spectra obtained from the sample milled for up to 20 h and that milled for 30 h. (c) Mechanism of luminescence of ruby excited with a green laser of 532 nm wavelength.

α-Cr:$Al_2O_3$ (in this case ruby) at room temperature. The $R_1$ and $R_2$ bands show a relatively high intensity, making the detection of the ruby phase in a few parts per millions possible, which is rather challenging by other methods. Therefore, Raman spectroscopy is a highly desirable method to characterize this phase. Detecting the bands $R_1$ and $R_2$ is essential because they are characteristic of the substitutional $Cr^{3+}$ ions that are unique to the substitution in the octahedral sites of α-$Al_2O_3$. Both the phase transformation and its successful identification in room temperature make this research unique.

Luminescence is an optical emission that involves the electron transitions between the states $^4A_2$ (ground state), $^4T_2$ (short lived state) and $^2E$ (metastable state) as explained in Fig. 3c. Fig. 3c shows the luminescence mechanism observed in the presence of an excitation line, *e.g.* 532 nm, and the emitted $R_1$ and $R_2$ bands. This may be explained in terms of crystal field theory, which dictates that the crystal field stabilization energy (CFSE) presents its maximum in the case of octahedral sites for d3 ($Cr^{3+}$).[35] Both bands, $R_1$ and $R_2$, are clearly discernible in all the milled samples and they are not present in the raw sample. The intensity of both bands increases with milling time and is proportional to the amount of ruby in the sample. To identify this phase, we need only 5 h of milling. The intensity of the peaks and their easy detection increase with time as well. This demonstrates the dynamic transformation from χ-$Al_2O_3$ into α-Cr:$Al_2O_3$.

The discernibility of the bands is related to the higher crystallinity of the solid solution. This, in parallel, translates into the extinction of the $A_{1g}$ mode of $Cr_2O_3$ (Fig. 2). On the other hand, χ-$Al_2O_3$ is gaining crystal quality as shown in Fig. 1. However, pure α-$Al_2O_3$ is untraceable unless it is doped with $Cr^{3+}$. Patra *et al.*[36] showed that the crystalline ruby strongly affects the shape of the luminescence bands $R_1$ and $R_2$. They also proposed that the substitutional $Cr^{3+}$ ions in the octahedral sites of the δ-$Al_2O_3$ and θ-$Al_2O_3$ phases do not generate the $R_1$ and $R_2$ resonant bands. Instead, they exhibit only a broad band.[36] This again demonstrates that we are producing ruby at room temperature by a new green and purely mechanical method.

In Fig. 3b, the intensities of the $R_1$ and $R_2$ lines as a function of the milling time are plotted. The observed behavior shows that the formation of the solid solution increases linearly until 20 h of milling. The intensity of the $R_1$ and $R_2$ bands increases abruptly (exponential) in the sample milled for 30 h. This increase is approximately 13 fold larger when compared with the sample milled for 20 h. Besides the fact that after 30 h the pseudoboehmite is rather untraceable by XRD and confirmed by Raman, we conclude that all the pseudoboehmite has transformed into χ-$Al_2O_3$ and α-Cr:$Al_2O_3$.

In Fig. 4, we present a micrograph obtained using high resolution transmission electron microscopy (HRTEM) of the sample milled for 30 h. The image shows a by-crystal framework clearly identifying both phases in the investigated sample: χ-$Al_2O_3$ and α-Cr:$Al_2O_3$. Furthermore, in HRTEM, we did not observe pseudoboehmite which is in agreement with the XRD and Raman results. This result further confirms the

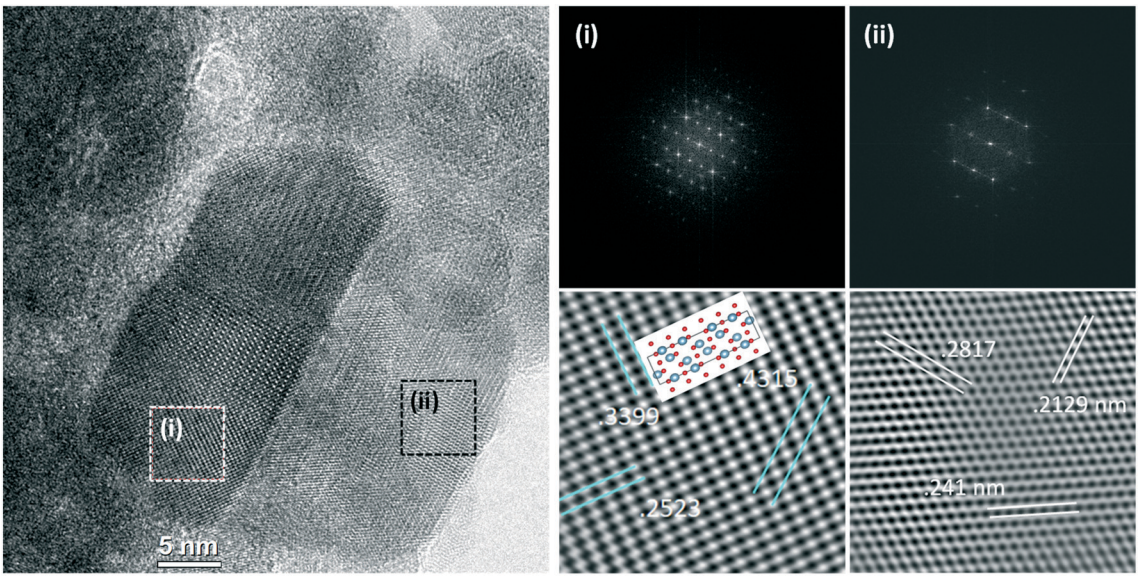


**Fig. 4** HRTEM images and interplanar measurements for α-Cr:$Al_2O_3$ (i) and χ-$Al_2O_3$ (ii) with the respective FFT images for each location showing the presence of each phase.

successful synthesis of α-Cr:$Al_2O_3$ by room temperature milling. The HRTEM micrographs also confirm that the sample is nanostructured. The presence of ruby under HRTEM is a clear demonstration of the potential of milling to synthesize ruby at room temperature.

The HRTEM image shows two main particles that are analyzed by means of FFT to produce their respective diffraction patterns. The FFT image is then converted into the IFFT to generate filtered and hence clearer images from the areas labeled (i) and (ii). The analysis of area (i) matches with the characteristics of α-$Al_2O_3$. On the other hand, area (ii) corresponds to χ-$Al_2O_3$. The inset in the IFFT image for (i) clearly matches with the simulated structure that is presented in the HRTEM image. Unfortunately, we cannot generate the same image for χ-$Al_2O_3$ because this phase is not well investigated and the space group of this phase has not been reported. The space group is fundamental to identify the actual crystalline structure and it is also mandatory in order to simulate the respective structures. It is known that χ-$Al_2O_3$ matches with the expected phase according to the JCPDS chart for χ-$Al_2O_3$. The results agree with XRD and Raman allowing us to confirm the room temperature synthesis of χ-$Al_2O_3$ and α-Cr:$Al_2O_3$.

Fig. 5 shows the thermal analysis results where the complete transformation to α-Cr:$Al_2O_3$ from the raw material and the sample milled for 30 h is monitored. The 30 h sample is used for this analysis to enhance the differences in phase transformations when compared to the raw sample. A major finding herein is the transformation of different phases during the annealing process for the raw and milled samples. The raw sample shows water evaporation and dehydroxylation along with transformation to δ-$Al_2O_3$, and then, α-Cr:$Al_2O_3$. The milled sample shows a combined endotherm for the water loss and dehydroxylation, which is followed by χ-$Al_2O_3$, κ-$Al_2O_3$ and finally α-Cr:$Al_2O_3$.

The heat flow profile of the raw sample has two endothermic reactions. The first for correspond to the sobbed water and the second is attributed to the dehydroxylation process. In the milled sample, we observe only one endothermic process that is associated with the combined process of dehydration and dehydroxylation. This represents a reduction in the energy requirements of 58% for the milled sample to transform into χ-$Al_2O_3$. At higher temperatures, the raw sample and the sample milled for 30 h show the presence of the following intermediate phases, δ-$Al_2O_3$ and κ-$Al_2O_3$. This phase identification is made based on the transformations reported in ref. 37 and 38. In both cases, as the temperature increases, the intermediate phases transform into α-Cr:$Al_2O_3$.

For the milled sample, the transformation to α-Cr:$Al_2O_3$ initiates at approximately 867 °C and concludes at 1163 °C. In the case of the raw sample, the same reaction initiates at 1060 °C and ends at 1190 °C. This represents a reduction in transformation temperature of approximately 193 °C which is attributed to presence of α-Cr:$Al_2O_3$ "seeds" that are

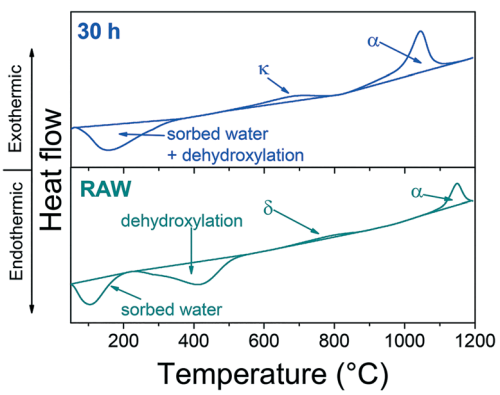


**Fig. 5** DSC analysis of raw and 30 h milled pseudoboehmite.

 

synthesized at room temperature by milling. The α-Cr:$Al_2O_3$ seeds are nanometric and act as hetero-nuclei for high-temperature α-Cr:$Al_2O_3$.

The energy requirements to transform κ- and δ-$Al_2O_3$ are exothermic, but in both cases, the energy released is almost negligible. On the other hand, the transformation to α-Cr:$Al_2O_3$ has a significantly larger exothermic reaction (Fig. 5). In a comparative analysis, the increase in the internal energy released during the transformation to α-Cr:$Al_2O_3$ is 285% larger in the milled sample. Therefore, this is clear evidence that milling is an α-Cr:$Al_2O_3$ promoter, allowing a less demanding phase transformation process. The energies are estimated as the areas under the curves between the heat curve and the base line identified in Fig. 5.

Fig. 6 shows the Raman spectra of the raw sample (pseudoboehmite) and the α-Cr:$Al_2O_3$ powder obtained after heat treatment. The resulting vibrational modes confirm the full transformation to α-Cr:$Al_2O_3$ which agrees with the XRD results. All the active vibrational modes for both pseudoboehmite and α-Cr:$Al_2O_3$ were successfully identified in the respective samples. Again, in the milled sample there is only a partial transformation to α-Cr:$Al_2O_3$ and it can only be detected by Raman spectroscopy through the $Cr_2O_3$ additions that are used to synthesize ruby. The presence of α-Cr:$Al_2O_3$ seeds is responsible for the synthesis of highly crystalline alumina even at temperatures of 193 °C, below the equilibrium temperature of this phase. This temperature drop is a quantum leap for optoelectronic applications as this opens the door to a wide variety of new substrates that can be coated with sapphire or ruby. Potential applications of this material include electronics, optics, aerospace, superconductivity, and biological use. As an example of potential applications, here we cite our previous work.[39] Based on the Raman spectra in Fig. 6, one can say that there is no evidence of any other phase except for α-Cr:$Al_2O_3$. Therefore, here we no longer need to analyze the ruby in the sample; instead, we characterize α-Cr:$Al_2O_3$ directly. Furthermore, our results were satisfactorily checked against the Bilbao Crystallographic Server.[34]

Fig. 7 shows an analysis of the shift on the luminescence lines $R_2$ and $R_1$ (compared with Fig. 3), which is associated

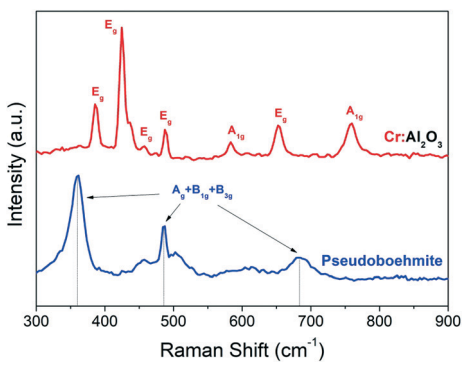


Fig. 6 Raman spectrum of pseudoboehmite and α-Cr:$Al_2O_3$ acquired with a laser source of 532 nm wavelength.

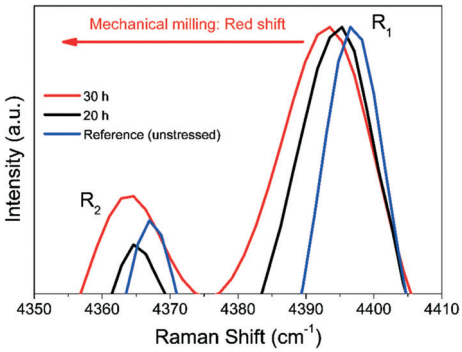


Fig. 7 Raman spectra of the samples milled for 20 h and 30 h against the unstressed sample (reference).

with compressive residual stress. The residual stress build up is an important factor that affects the performance of structural materials such as protective oxide barriers, thermal coatings and bulk materials. In the literature, we can find several studies about the estimation of the residual stresses for different systems, not only for barriers and coatings but also for bulk materials.[40,41] However, here we use this parameter to assess the level of residual stresses as a measure of internal energy increase. Here we present the results for the samples milled for 20 and 30 h and we compare the results to a reference sample. The reference sample was produced by annealing pure pseudoboehmite + 0.2$Cr_2O_3$ at 1300 °C for 2 h. The conditions were set for the lowest temperature and the shortest time capable of producing samples where the $R_1$ and $R_2$ bands are no longer shifting (zero-residual stress). At the same time, this prevents excessive grain growth. This annealing is also sufficient to fully develop the solid solution (α-Cr:$Al_2O_3$) between α-$Al_2O_3$ and $Cr_2O_3$.

The relative change in residual stresses is used as an indirect measure of the changes in internal energy in the sample. The residual stresses attributed to the substitution of $Cr^{3+}$ for $Al^{3+}$ in octahedral sites contribute to the compressive state of the sample. However, this contribution is rather limited because the sample composition in both cases is similar and it is only 0.2 wt%. Therefore, the main component here is the residual stresses due to milling. In the reference sample, the $R_2$ and $R_1$ bands were identified at 4367.3 $cm^{-1}$ and 4397.0 $cm^{-1}$, respectively.

The longer the milling time, the better define the resonant bands, due to an increase in the ruby phase. This in turn improves the resolution and accuracy of the Raman analysis. For the $R_1$ band (higher intensity),[42] the red shift ($\Delta R_1$) for the sample milled for 20 h is = 2.8 $cm^{-1}$ and for 30 h is = 4.2 $cm^{-1}$. Using eqn (1), we calculated the respective compressive stresses

$$\Delta\nu = -7.59P \quad (1)$$

where $\Delta\nu$ is the change of frequency in $cm^{-1}$, $P$ is the pressure in GPa and −7.59 is the piezo-spectroscopic constant. The calculated values are −0.37 GPa and −0.55 GPa for the

samples milled for 20 and 30 h, respectively. The increase in residual stress is in agreement with the increase in internal energy as presented in the Thermal analysis section. Therefore, this is a sort of measure of off-equilibrium conditions that contributed to the drop in transformation temperature to α-Cr:$Al_2O_3$ as well as the energy requirements for the full transformation to α-Cr:$Al_2O_3$. In conclusion, the increase in internal energy promotes the transformation at lower temperatures and a higher exothermic release for the phase transformation.

# Conclusion

In the present work, the successful synthesis of χ-$Al_2O_3$ and α-Cr:$Al_2O_3$ at room temperature is demonstrated. This is possible by means of mechanical milling of pseudoboehmite. The additions of $Cr_2O_3$ are the key to successfully identifying the synthesized ruby by means of Raman spectroscopy. Mechanical milling supplies sufficient energy to promote partial dehydration and dehydroxylation to synthesize χ-$Al_2O_3$ along with the substitution of $Cr^{3+}$ in octahedral sites, typical of $Al^{3+}$. Here we reported that pseudoboehmite starts to transform to χ-$Al_2O_3$ at times as short as 20 h of milling. However, α-Cr:$Al_2O_3$ or ruby transformation is observed in milling times as low as 5 h and it is traceable with Raman. Due to the limited amounts of ruby, this phase is untraceable by any other method, except for HRTEM. Thermal analysis suggests a new synthesis route to produce ruby after heat treatment as well as a reduction in the transformation temperature of α-Cr:$Al_2O_3$ of approximately 193 °C after 30 h of milling. This temperature drop is attributed to the α-Cr:$Al_2O_3$ hetero-nuclei that are synthesized during milling as well as the increase in internal energy.

# Materials and methods

### Synthesis of pseudoboehmite

The pseudoboehmite was synthesized from a 0.2 M water based aluminum sulfate ($Al_2(SO_4)_3{\cdot}xH_2O$, purity ≥ 98% from Sigma Aldrich) solution. The solution was heated to 60 °C with vigorous stirring under additions of ammonia ($NH_3$) gas. The solution is kept at a constant pH (pH = 9–10) through the entire precipitation process. Eqn (2) and (3) represent the precipitation process. At the end of the reaction, the products obtained are filtered and washed with distilled water for a number of times. The washing process is ended when the washing solution has a constant pH of 7. The resulting product is dried at 100 °C for 24 h. The larger particles are then pulverized in a mortar to obtain a white and loose powder. The product is our raw material known as pseudoboehmite.

$$NH_3 + H_2O \rightarrow NH_4^+ + OH^- \quad (2)$$

$$2Al^{3+} + 3SO_4^{2-} + 6NH_4^+ + 6OH^- \rightarrow 2AlO(OH) + 2H_2O + 3(NH_4)_2SO_4 \quad (3)$$

### Mechanical milling

Pseudoboehmite powders were mixed with chromium oxide ($Cr_2O_3$, purity ≥ 98% from Sigma Aldrich). The weight ratio of pseudoboehmite and $Cr_2O_3$ was 99.8 : 0.2% wt. Batches of 10 grams were milled into a stainless steel Spex media for up to 30 h.

### Thermal analysis

The thermal analysis was performed using a SETARAM differential scanning calorimeter (DSC) analyzer . The raw and 30 h milled powders were analyzed at a heating rate of 15 °C $min^{-1}$ up to a maximum temperature of 1200 °C in an argon atmosphere.

### Structural characterization

Characterization was carried out by means of XRD (X-ray diffraction) using a Siemens D5000 diffractometer with a Bragg–Brentano geometry and Cu-Kα radiation ($\lambda$ = 1.5418 Å). Raman spectroscopy was conducted using a confocal micro-Raman microscope (Xplora™, Horiba JY). A 532 nm diode laser was used for excitation. High-resolution transmission electron microscopy (HRTEM) was performed using a transmission electron microscope (JEM-2200FS JEOL) operated at 200 kV. The image analysis for the HRTEM micrographs is conducted using Digital Micrograph that is capable of reproducing the fast Fourier transformation (FFT) and their inverse (IFFT) images for a more in-depth analysis.

# Conflicts of interest

There are no conflicts of interest.

# Acknowledgements

Both, FCRH and FCV, wish to acknowledge CONACyT-Mexico for the support given to FCV to pursue his PhD studies and obtain research experience and for the financial support to participate in the research exchange program at the University of Houston. SRB acknowledges financial support from the National Science Foundation under the contract CHE 1605331 and the University of Houston GEAR 2013 program.

# References

1 M. Trueba and S. P. Trasatti, *Eur. J. Inorg. Chem.*, 2005, 3393–3403.
2 D. L. Trimm and A. Stanislaus, *Appl. Catal.*, 1986, **21**, 215–238.
3 H. Masuda, H. Asoh, M. Watanabe, K. Nishio, M. Nakao and T. Tamamura, *Adv. Mater.*, 2001, **13**, 189–192.
4 A. Kurella and N. B. Dahotre, *J. Biomater. Appl.*, 2005, **20**, 5–50.
5 S. Chang, R. H. Doremus, L. S. Schadler and R. W. Siegel, *Int. J. Appl. Ceram. Technol.*, 2004, **1**, 172–179.

 

6 S. Sōmiya and M. Kaneno, in *Handbook of advanced ceramics materials, applications, processing, and properties*, Academic Press, Amsterdam, 2013, pp. pages cm.
7 S. Somiya, in *Handbook of Advanced Ceramics*, Elsevier Ebsco Publishing [Distributor], New York Ipswich, 2003.
8 N. P. Bansal, *American Ceramic Society., in: Ceramic transactions; v. 220*, John Wiley; American Ceramic Society, Hoboken, N. J. [Westerville, Ohio], 2010, pp. ix, 312 p.
9 A. Z. A. Azhar, L. C. Choong, H. Mohamed, M. M. Ratnam and Z. A. Ahmad, *J. Alloys Compd.*, 2012, **513**, 91–96.
10 A. Pillonnet, C. Garapon, C. Champeaux, C. Bovier, H. Jaffrezic and J. Mugnier, *J. Lumin.*, 2000, **87–89**, 1087–1089.
11 T. H. Maiman, *Nature*, 1960, **187**, 493–494.
12 J. W. Huang and H. W. Moos, *Phys. Rev.*, 1968, **173**, 440–444.
13 K. Syassen, *High Pressure Res.*, 2008, **28**, 75–126.
14 B. R. Jovanic, *Chem. Phys. Lett.*, 1992, **190**, 440–442.
15 H. K. Mao, J. Xu and P. M. Bell, *J. Geophys. Res., [Solid Earth Planets]*, 1986, **91**, 4673–4676.
16 D. P. Ma, X. T. Zheng, Y. S. Xu and Z. G. Zhang, *Phys. Lett. A*, 1986, **115**, 245–248.
17 I. Fujishiro, Y. Nakamura, T. Kawase and B. Okai, *JSME Int. J., Ser. I*, 1988, **31**, 136–141.
18 Z. R. Zhang and T. J. Pinnavaia, *Angew. Chem., Int. Ed.*, 2008, **47**, 7501–7504.
19 S. Zhang, K. A. Khor and L. Lu, *J. Mater. Process. Technol.*, 1995, **48**, 779–784.
20 H. A. Calderon, I. Estrada-Guel, F. Alvarez-Ramírez, V. G. Hadjiev and F. C. Robles Hernandez, *Carbon*, 2016, **102**, 288–296.
21 F. Robles-Hernández and H. Calderón, in: *ICCE-16 Conference*, Kunming, China, 2008.
22 I. I. Santana, F. C. Robles Hernandez, V. Garibay Febles and H. A. Calderon, *Solid State Phenom.*, 2011, **172–174**, 727–732.
23 J. S. Benjamin, *Powder Metall. Int.*, 1980, **12**, 43.
24 J. S. Benjamin, *Mater. Sci. Forum*, 1992, **88**, 1–17.
25 P. S. Gilman and J. S. Benjamin, *Annu. Rev. Mater. Sci.*, 1983, **13**, 279–300.
26 C. Suryanarayana, *Prog. Mater. Sci.*, 2001, **46**, 1–184.
27 W. N. Martens, R. L. Frost, J. Bartlett and J. T. Kloprogge, *J. Mater. Chem.*, 2001, **11**, 1681–1686.
28 B. R. Baker and R. M. Pearson, *J. Catal.*, 1974, **33**, 265–278.
29 R. Tettenhorst and D. A. Hofmann, *Clays Clay Miner.*, 1980, **28**, 373–380.
30 Y. Geng, T. Ablekim, P. Mukherjee, M. Weber, K. Lynn and J. E. Shield, *J. Non-Cryst. Solids*, 2014, **404**, 140–144.
31 A. K. Giri, *Adv. Mater.*, 1997, **9**, 163–166.
32 F. Q. Guo and K. Lu, *Metall. Mater. Trans. A*, 1997, **28**, 1123–1131.
33 T. Kozawa and M. Naito, *Adv. Powder Technol.*, 2016, **27**, 935–939.
34 E. Kroumova, M. I. Aroyo, J. M. Perez-Mato, A. Kirov, C. Capillas, S. Ivantchev and H. Wondratschek, *Phase Transitions*, 2003, **76**, 155–170.
35 A. Rastorguev, M. Baronskiy, A. Zhuzhgov, A. Kostyukov, O. Krivoruchko and V. Snytnikov, *RSC Adv.*, 2015, **5**, 5686–5694.
36 A. Patra, R. E. Tallman and B. A. Weinstein, *Opt. Mater.*, 2005, **27**, 1396–1401.
37 P. S. Santos, H. S. Santos and S. P. Toledo, *Mater. Res.*, 2000, **3**, 104–114.
38 G. W. Brindley, *Am. Mineral.*, 1961, **46**, 14.
39 F. D. C. Vega, P. G. M. Torres, J. P. Molina, N. M. G. Ortiz, V. G. Hadjiev, J. Z. Medinaa and F. C. R. Hernandez, *J. Mater. Chem. C*, 2017, **5**, 4959–4966.
40 J. K. Odusote, L. A. Cornish, L. H. Chown and R. M. Erasmus, *Corros. Sci.*, 2013, **70**, 276–284.
41 L. Y. Yang, L. Zheng and H. B. Guo, *Corros. Sci.*, 2016, **112**, 542–551.
42 G. K. Banini, M. M. Chaudhri, T. Smith and I. P. Hayward, *J. Phys. D: Appl. Phys.*, 2001, **34**, L122.